



EUROPEAN
COMMISSION

European
Research Area

Carbon-14 Source Term

CAST



¹⁴CAST

Report on corrosion behaviour of stainless steel (D2.12)

Author(s):

T. Sakuragi

Date of issue of this report: 07/07/2017

The project has received funding from the European Union's European Atomic Energy Community's (Euratom) Seventh Framework Programme FP7/2007-2013 under grant agreement no. 604779, the CAST project.		
Dissemination Level		
PU	Public	X
RE	Restricted to the partners of the CAST project	
CO	Confidential, only for specific distribution list defined on this document	



CAST – Project Overview

The CAST project (CARbon-14 Source Term) aims to develop understanding of the potential release mechanisms of carbon-14 from radioactive waste materials under conditions relevant to waste packaging and disposal to underground geological disposal facilities. The project focuses on the release of carbon-14 as dissolved and gaseous species from irradiated metals (steels, Zircalloys), irradiated graphite and from ion-exchange materials as dissolved and gaseous species.

The CAST consortium brings together 33 partners with a range of skills and competencies in the management of radioactive wastes containing carbon-14, geological disposal research, safety case development and experimental work on gas generation. The consortium consists of national waste management organisations, research institutes, universities and commercial organisations.

The objectives of the CAST project are to gain new scientific understanding of the rate of re-lease of carbon-14 from the corrosion of irradiated steels and Zircalloys and from the leaching of ion-exchange resins and irradiated graphites under geological disposal conditions, its speciation and how these relate to carbon-14 inventory and aqueous conditions. These results will be evaluated in the context of national safety assessments and disseminated to interested stakeholders. The new understanding should be of relevance to national safety assessment stakeholders and will also provide an opportunity for training for early career researchers.

For more information, please visit the CAST website at:

<http://www.projectcast.eu>

CAST		
Work Package: 2	CAST Document no. :	Document type:
Task: 2.3	CAST-2017-D2.12	R
Issued by: RWMC		Document status:
Internal no. :		Final

Document title
Report on corrosion behaviour of stainless steel

Executive Summary

RWMC has been studied the aqueous corrosion of non-irradiated stainless steel under the simulated repository conditions. The sensitive hydrogen measurement was selected to obtain the very low corrosion rate of stainless steel based on a reaction of $3\text{Fe} + 4\text{H}_2\text{O} \rightarrow \text{Fe}_3\text{O}_4 + 4\text{H}_2$. Two experimental systems have been applied; the glass ampoule method which is a batch type measurement for short term at elevated temperatures up to 353 K, and the gas flow system which monitors the hydrogen gas continuously for a long term over 6 years at a constant temperature. The selected solution is basically a dilute NaOH solution of pH 12.5 and a pure water for comparison and a fundamental study.

Our long term observation for the corrosion behaviour was demonstrated that the corrosion rate decreases with time during the initial first year. After that the corrosion rate is constant over 6.5 years of which value was approximately 0.4 nm/y at 303 K. This corrosion rate increases with rising temperature. The corrosion behaviour in pure water and NaOH solution is comparable. The detailed kinetics in the initial behaviour is suggested that the stainless steel corrosion follows a parabolic rate law, which suggested the corrosion process is under diffusion control. The activation energy is determined to be 82.5 ± 6.2 kJ/mol. The characterisation of surface oxide after corrosion by TEM together with EDX and electron diffraction measurements. The oxide of several nm thick considered to be a passive film is amorphous and is consisted from Fe, Cr and Ni.

List of Contents

Executive Summary	i
List of Contents	ii
1 Introduction	1
2 Materials and Methods	3
2.1 Specimen Characteristics	3
2.2 Batch Ampoule Experiment	3
2.3 Gas Flow Experiment	5
3 Results and Discussion	5
3.1 Corrosion Rate	5
3.2 Short Term Kinetic Behaviour in NaOH Solution	8
3.3 Characteristics of Surface Oxide	12
4 Conclusion	15
Acknowledgement	16
References	16

1 Introduction

Spent fuel assemblies comprising stainless steel are expected to be disposed of in an underground repository (Figure 1.1.1). Carbon 14 is a typical activated product in metallic wastes and is mainly generated by the $^{14}\text{N}(n,p)^{14}\text{C}$ reaction. For the waste in Japan as shown in Figure 1.1.2 it has been assumed that the stainless steel nozzles account for 16% by weight of the spent assembly waste, and their C-14 corresponds to 27.5% of the total ^{14}C inventory of 4.5×10^{14} Bq [SAKURAGI *et al.*, 2013]. The corrosion phenomenon is considered to be a leaching source of activated radionuclides such as ^{14}C . The corrosion behaviour of stainless steels under anticorrosive repository conditions (low oxygen, high alkaline, and in situ temperature under 353 K) has been consequently outstanding, in large part because the corrosion rate is too small to be clearly comprehended by common methods [IAEA, 1998]. Japanese safety assessment has estimated the corrosion rate of stainless steel as 20 nm per year based on limited experimental result at 308 K in the presence of 3,200 ppm chloride, which corresponds to its leaching periods of 8,400 years [FEPEC and JAEA, 2007]. Other countries also estimate the comparable corrosion rate [SWNTON *et al.*, 2015]

The purpose of this report is to show the long-term corrosion behaviour of the austenitic stainless steel under deoxygenated conditions. A high pH solution (NaOH) was selected to simulate the typical underground repository environment and deionized water was selected to understand fundamentally the corrosion behavior. We have employed two experimental setups to measure sensitively the hydrogen gas from the corrosion reaction that can be applied to the extremely slow corrosion rate of stainless steel. The batch ampoule method was applied to relatively short-term tests and for the tests at different temperatures up to 353 K. The gas flow experiment that can monitor the evolved hydrogen continuously was applied to a long-term behaviour over 6 years under a constant temperature. The corrosion process is then discussed with activation energy and oxide characteristics.

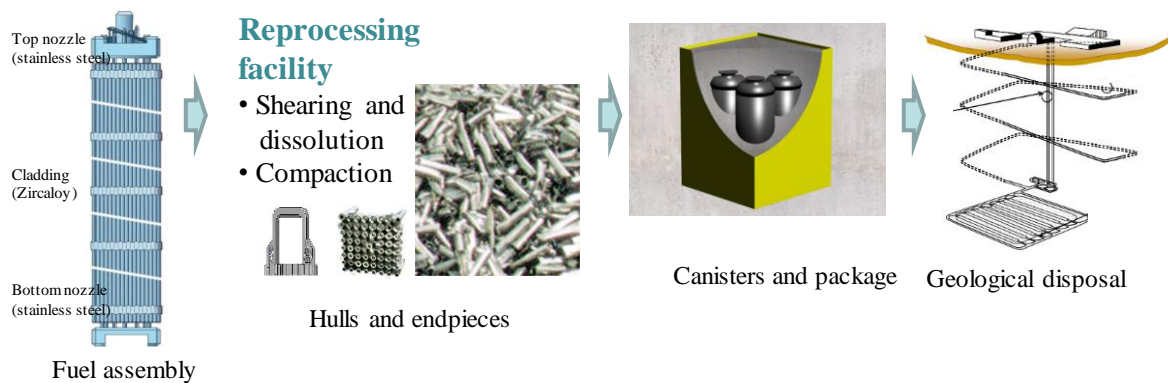


Figure 1.1.1: Generation and disposal concept of activated metallic waste in Japan.

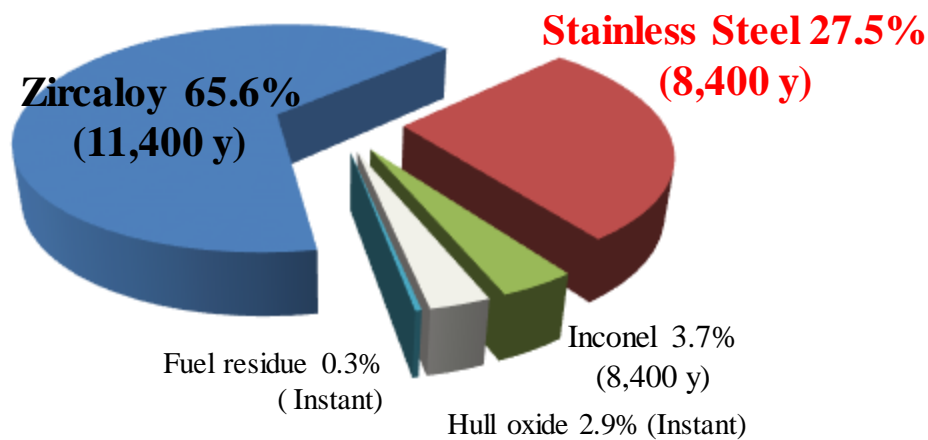


Figure 1.1.2: C-14 inventory for spent fuel assemblies corresponding to commercial 32,000 MTU reprocessing in Japan [SAKURAGI et al., 2013]. The values in parentheses represent the assumed leaching period in the Japanese safety assessment [FEPEC and JAEA, 2007].

2 Materials and Methods

2.1 Specimen Characteristics

The 18Cr-8Ni austenitic stainless steel with a thickness of 0.1 mm was obtained from Nilaco Corporation (Product No. 753323). The chemical composition is shown in Table 2.1.1. The stainless steel sheet was polished with 0.02 mm alumina powder and then cut to the appropriate size. Figure 2.1.1 shows the surface condition before the corrosion test. The average diameter of the grains was approximately 15 μm , and the initial oxide thickness was approximately 3 nm.

Table 2.1.1: Chemical compositions of 18Cr-8Ni austenitic stainless steel (wt%)

	C	Si	Mn	P	S	Ni	Cr	H(ppm)
Specification	<0.08	<1.00	<2.00	<0.045	<0.030	8.00-10.50	18.00-20.00	-
Specimen	0.07	0.45	0.79	0.028	0.005	8.29	18.14	-

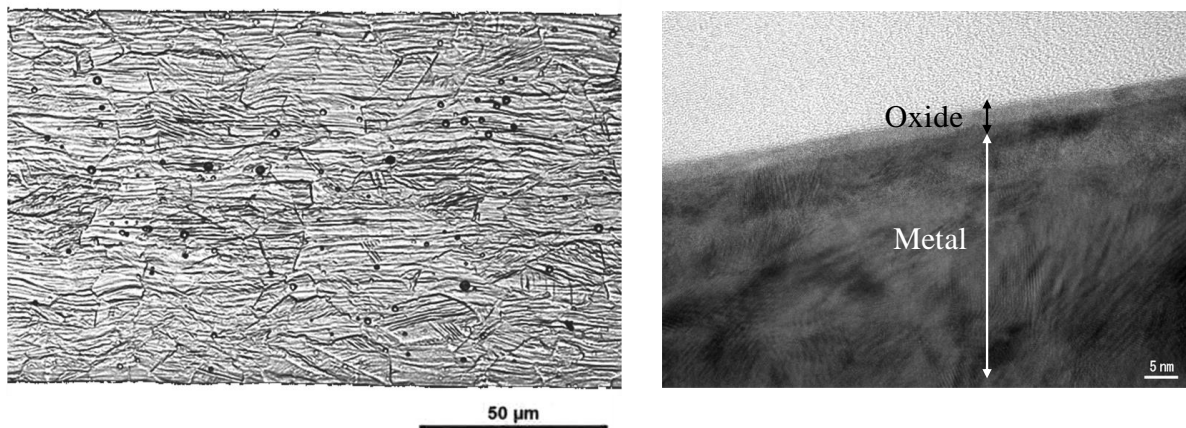


Figure 2.1.1: Optical micrograph of a chemically etched cross-section of stainless steel (left) and TEM observation of the surface oxide before immersion (right).

2.2 Batch Ampoule Experiment

An ampoule batch test was performed according to the methods developed by Honda et al. [HONDA *et al.*, 1999], and the test procedure is presented in Figure 2.2.1. The stainless

steel strips (22 pieces; 3 mm×90 mm×0.1 mm, surface area of $1.19 \times 10^{-2} \text{ m}^2$) were set in glass ampoules. A stop-cock was attached, then the ampoule was filled with an appropriate solution (deionised water or dilute NaOH solution of pH 12.5) and the stop-cock closed. This enclosure procedure was performed in a glove box that had been purged by nitrogen gas with oxygen concentration below 0.1 ppm. The ampoules were moved outside the glove box and sealed by heating. After the corrosion periods under controlled temperatures, the ampoules were set on a vacuum gas collection system that connected to gas chromatography equipment and the hydrogen gas was measured.

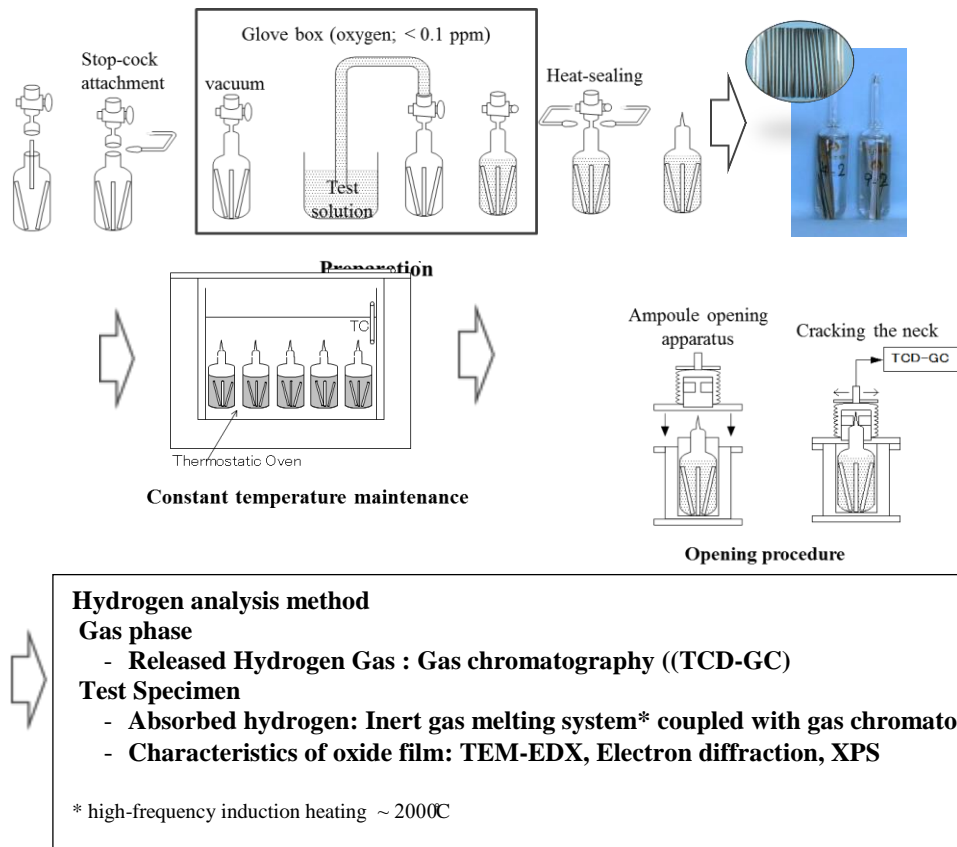


Figure 2.2.1: Procedure for ampoule batch corrosion experiment.

2.3 Gas Flow Experiment

The experimental setup for the gas flow corrosion system is shown in Figure 2.3.1. This system can monitor the generated hydrogen gas continuously. The stainless steel samples (20 sheets; 100 mm×100 mm×0.1 mm, surface area of 0.40 m²) were immersed in 2.5 dm³ of deoxygenated deionised water or dilute NaOH solution (initial pH = 12.5). An argon carrier gas was passed through the inner flask, and the hydrogen concentration in the carrier gas was measured periodically using atmospheric pressure ionization mass spectrometry (API-MS, Hitachi Tokyo Electronics, UG-400). Hydrogen contamination from the atmosphere (approximately 0.5 ppm) and also oxygen was avoided by using a double container system. Several test vessels were prepared together with a vessel of a blank test.

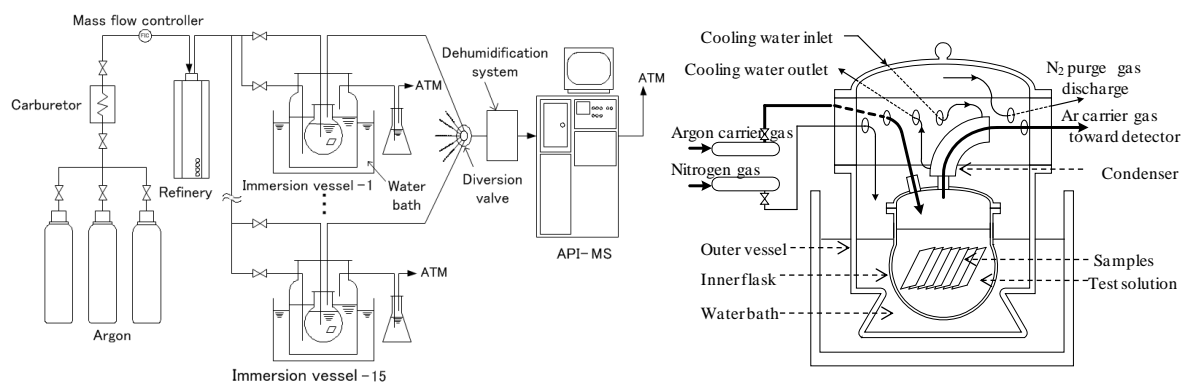
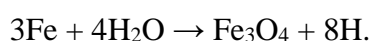


Figure 2.3.1: Overview of the gas flow experimental system (left) and detailed illustration of the immersion vessel (right).

3 Results and Discussion

3.1 Corrosion Rate

The corrosion rate of the stainless steel can be obtained by assuming the following corrosion reaction:



Because hydrogen absorption into the metal is negligible (measured less than 3% [SAKURAGI *et al.*, 2016 a]), the corrosion rate R_c (nm/year), which represents the amount of iron consumed by oxidation under the stoichiometry in the above reaction, can be obtained from gaseous hydrogen as

$$R_c = \frac{3}{8} \cdot \frac{A_{\text{gas}} \cdot M_{\text{Fe}} \cdot 10^9}{\rho_{\text{Fe}} \cdot t},$$

where A_{gas} is the atomic molar amount of gaseous hydrogen per unit surface area (mol/m²), M_{Fe} is the molecular weight of iron (55.85 g/mol), ρ is the iron density (7.87×10^6 g/m³), and t is the test time in years.

For the glass ampoule method, the A_{gas} can be obtained directly from the hydrogen gas concentration in the ampoule. On the other hand, the cumulative A_{gas} from the gas flow experiment of consecutive measurements of hydrogen gas can be obtained from

$$A_{\text{gas}} = \frac{2}{S} \sum \frac{C_{t_i} + C_{t_{i-1}}}{2} \cdot \frac{v}{V^\circ} \cdot (t_i - t_{i-1}),$$

where C_{t_i} is the net concentration of H₂ gas (ppb) at time t_i , t_{i-1} is one time increment before t_i , v is the gas flow rate (0.9 dm³/min.), V° is the molar volume of a perfect gas (22.4 dm³/mol), and S is the surface area (0.4 m²).

Figure 3.1.1. shows the hydrogen gas concentration in the argon carrier gas of the gas flow system. In the dilute NaOH solution, the C_t values decreased over time from 15 to 1.5 ppb in the initial year. After that the hydrogen concentration can be considered to be constant: average values of Run 1 and Run 2 are 1.50 ± 0.34 ppb and 1.67 ± 0.42 ppb, respectively. This amount is adequate for the blank test (0.32 ± 0.06 ppb). Similar trends can be seen in the deionized water but the slight lower C_t values than that in NaOH solution may be attributed to the temperature difference of 5°C.

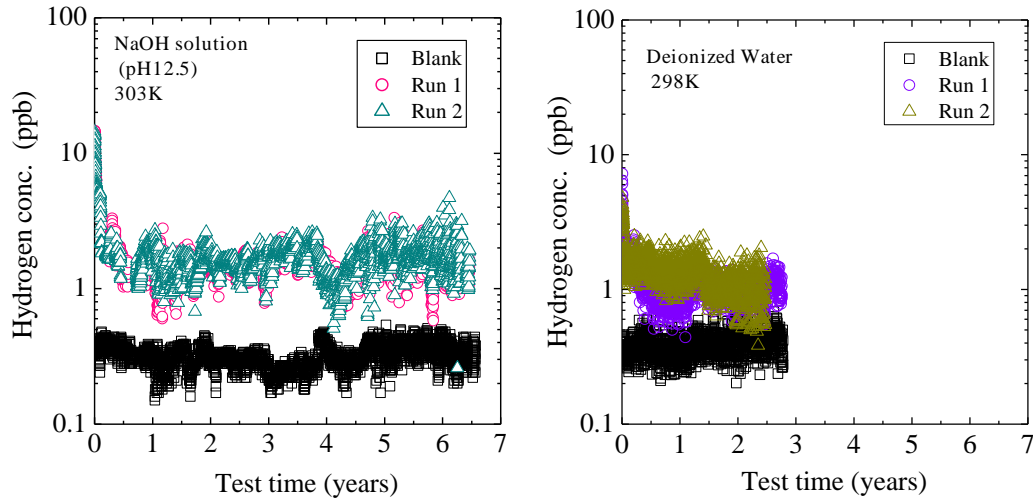


Figure 3.1.1: Gaseous hydrogen concentration generated from stainless steel in the gas flow system. Left represents the data in a dilute NaOH solution of pH 12.5 at 303 K [SAKURAGI et al., 2016 a]. Right represents the data in deionized water at 298 K.

Figure 3.1.2. shows the corrosion rate of stainless steel calculated by the two methods of hydrogen measurement in a NaOH and deionized water up to 353 K. The R_c values decrease with time over the first year and seem to be constant after that. The average value after one year is approximately 0.4 nm/y by the gas flow method in NaOH solution at 303 K. A similar trend has been obtained in the deionized water but the slight lower R_c values than that in NaOH solution for the gas flow system may be attributed to the temperature difference of 5°C as mentioned above. For the batch ampoule test, the the R_c values increase at increasing temperature. We will discuss the temperature effect on kinetics at the following section in detail.

The R_c values in the ampoule tests show slightly larger corrosion rates than that obtained by the gas flow system. This difference in results according to the experimental method was also observed for the corrosion of zirconium alloys [SAKURAGI *et al.*, 2012, WP3 report (D3.19)]. Generally, unpolished metals show a trend of rapid corrosion. This result may be attributable to the fact that the surface area of the unpolished edge was a larger ratio of the

specimen area for the batch ampoule test (thin strips) than for the gas flow test (100 mm square foils).

In conclusion, these corrosion rates are lower than the rate used in the conventional evaluation in Japan of $R_c = 20 \text{ nm/y}$ (TRU-2 report) [FEPEC and JAEA, 2007] and have an impact on estimation of radionuclide leaching and gas generation in the safety assessment for disposal of stainless steel waste.

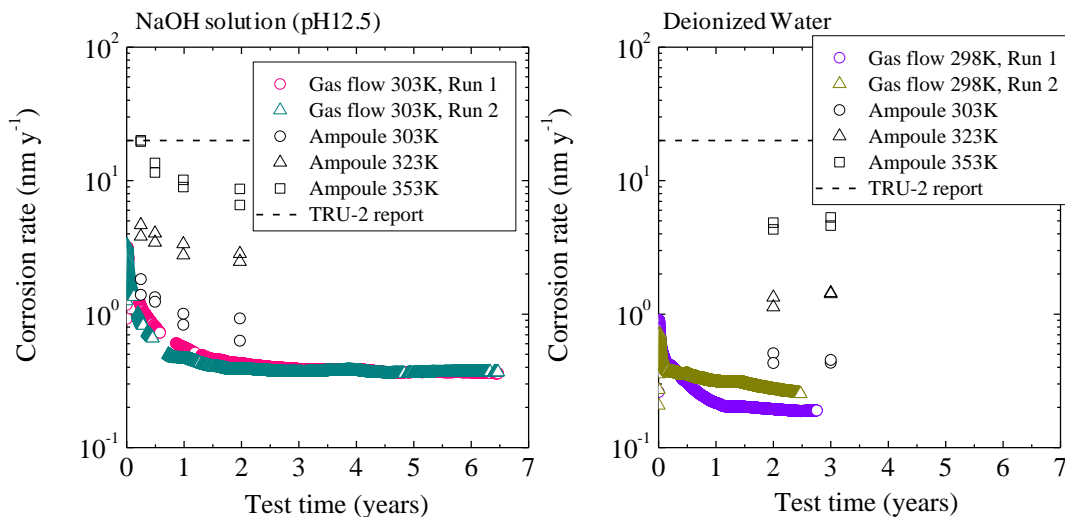


Figure 3.1.2: Corrosion rate of stainless steel as a function of time and temperature obtained. Left represents the data in a dilute NaOH solution of pH 12.5 by the gas flow method [SAKURAGI et al., 2016a] and by the glass ampoule method [SAKURAGI et al., 2016 b]. Right represents the data in deionized water. The dashed line is the assumption in a Japanese safety case (TRU-2 report) [FEPEC and JAEA, 2007].

3.2 Short Term Kinetic Behaviour in NaOH Solution

The kinetic behaviour of the aqueous corrosion of stainless steel has been discussed by Robertson for high temperatures down to 423 K together with a summary of parabolic corrosion rate constants [ROBERTSON, 1991]. At high temperature, the formation of duplex oxide on a metal surface and the diffusion of Fe ions through the oxide are considered to be rate controlling for the corrosion.

As shown in Figure 3.2.1, the hydrogen gas generation at 303 K in the gas flow system shows a good parabolic relationship with time up to one year. After this first period the kinetic behaviour changes into a linear relationship that holds for time up to 6.5 years. Therefore, we will discuss the low temperature kinetics of stainless steel corrosion using data up to one year in the temperature range between 303 K to 353 K obtained from the batch ampoule tests in a dilute NaOH solution of pH 12.5 as following.

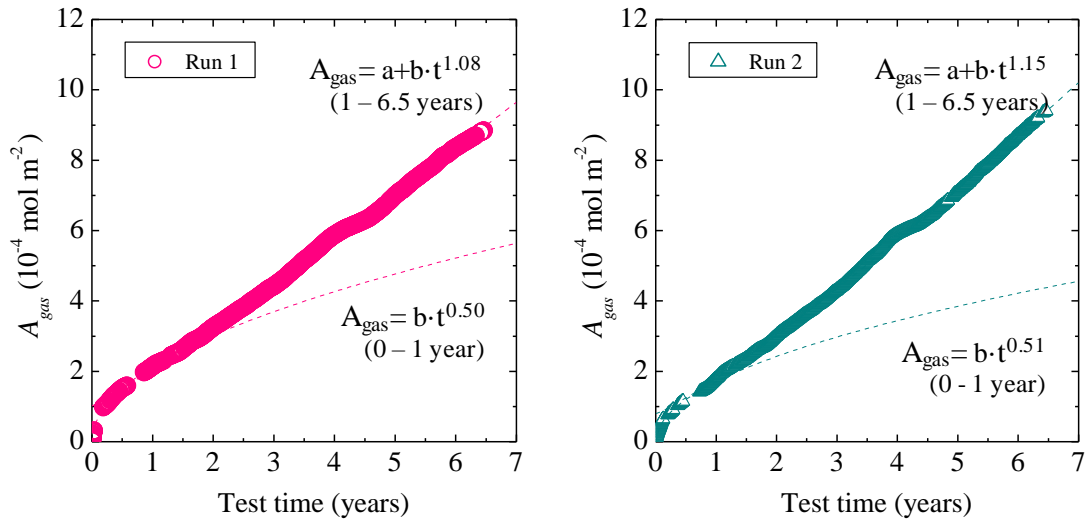


Figure 3.2.1: Amount of hydrogen as a function of corrosion time for the gas flow system in an NaOH solution. Dashed lines are best fitted curves.

The parabolic corrosion rate constants, k_p (cm²·sec⁻¹) can be obtained from the following equation [ATOKINSON, 1985 and ROBERTSON, 1991].

$$x^2 = k_p \cdot t,$$

$$k_p = a \cdot \exp\left(\frac{E_a}{RT}\right),$$

where x is the thickness (cm) of magnetite, Fe₃O₄, t is the test time (sec), a is a constant, E_a is the activation energy (kJ/mol), R is the universal gas constant (8.31 J/mol K), and T is the absolute temperature (K). Note that the x value used by Robertson was the total thickness of metal loss originally obtained by Maekawa et al. using A304 austenitic stainless steels in

neutral, de-aerated, and stationary water in the temperature range from 423 K to 633 K [MAEKAWA *et al.* 1968]. In the hydrogen measurement, the thickness of magnetite x can be calculated by the following equation, based on the assumed corrosion reaction.

$$x = \frac{1}{8} \cdot \frac{M_{\text{Fe}_3\text{O}_4} \cdot A_{\text{gas}}}{\rho_{\text{Fe}_3\text{O}_4}} \cdot 100,$$

where $M_{\text{Fe}_3\text{O}_4}$ and $\rho_{\text{Fe}_3\text{O}_4}$ are the molecular weight ($231.55 \text{ g}\cdot\text{mol}^{-1}$) and density ($5.2 \times 10^6 \text{ g}\cdot\text{m}^{-3}$) of magnetite. Figure 3.2.2 summarizes the relationship between x and time according to above equation. The corrosion kinetics obtained from the ampoule tests also exhibit a parabolic rate relationship fairly well.

Figure 3.2.3 shows the Arrhenius relationship of the parabolic rate constant (k_p) of stainless steel corrosion together with the high temperature data down to 423 K [MAEKAWA *et al.* 1968]. The k_p values in the present study are larger than those extrapolated from the data by Maekawa *et al.* The activation energy has been determined and found to be $82.5 \pm 6.2 \text{ kJ/mol}$, which corresponds to the value of $74.4 \pm 6.0 \text{ kJ/mol}$ that is shown under high temperatures down to 423 K. This result suggests that the basic corrosion mechanism is similar at both high and low temperatures. As mentioned above, the kinetic behaviour of aqueous corrosion of stainless steel at high temperature has been discussed by Robertson [ROBERTSON, 1991], who explained that the formation of duplex oxide on a metal surface and the diffusion of Fe ions through the oxide are considered to be rate controlling for the corrosion. The oxide characteristics formed under low temperature are discussed in the next section.

From the perspective of long-term safety, it is notable that the high temperature behaviour, when regarded as an acceleration test against the extremely slow corrosion at low temperatures, will facilitate good estimation for the eventual state of stainless steel waste after disposal. As shown previously in Figures 3.1.2 and 3.2.1, however, the corrosion kinetics of stainless steel after one year is suggested to change into a linear rate law that holds for time up to 6.5 years. The long-term behaviour is a major concern for the disposal

safety. It is a future challenge to understand the rate controlling process regarding the region of the linear relationship.

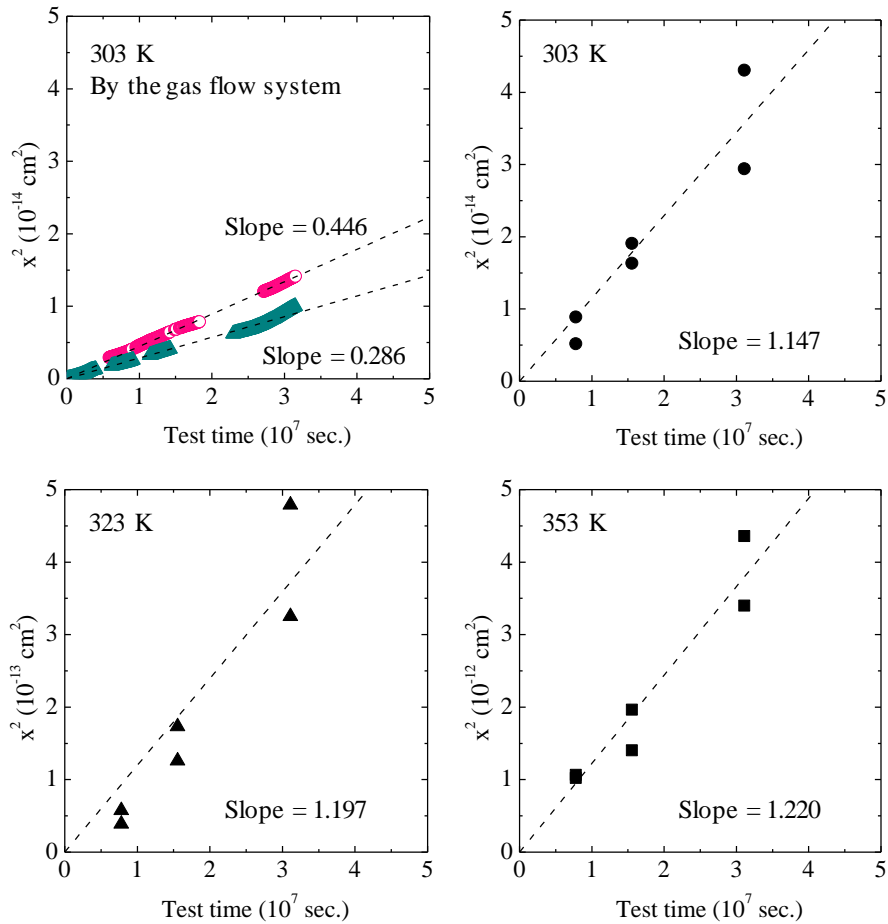


Figure 3.2.2: The relationship between square root of oxide thickness and test time. Lines are the linear regressions [SAKURAGI et al., 2016b].

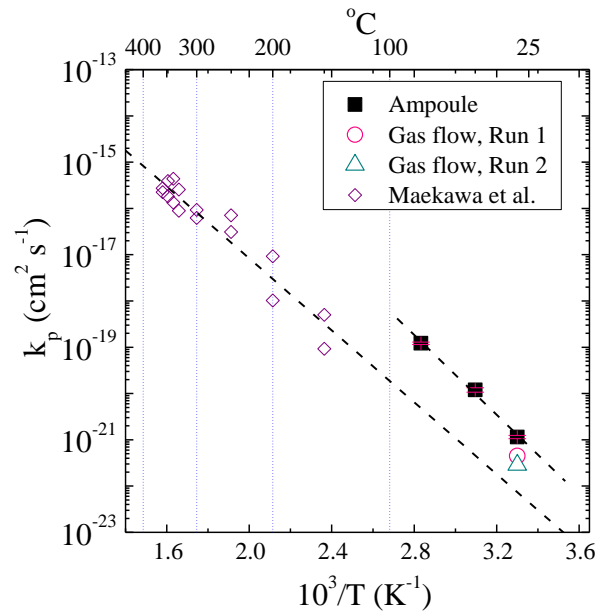


Figure 3.2.3: The parabolic rate constants of stainless steel corrosion. Dashed lines are least square fits [SAKURAGI et al., 2016 b].

3.3 Characteristics of Surface Oxide

Figure 3.3.1 shows the surface oxide observation by TEM formed at different temperatures after 2 years of immersion in the NaOH solution. The oxide film becomes thicker at increasing temperature. Table 3.3.1 summarizes the oxide thickness data obtained by TEM together with the magnetite thickness x calculated from hydrogen generation (A_{gas}) described in the above section. At 303 K, the increase in the thickness of this oxide portion from the initial value of 3 nm is negligible. At 323 K, the oxide thickness slightly increases with corrosion time. The rise in temperature also affects oxide growth. The magnetite layer is slightly thicker than that seen in TEM. It is possible that a part of magnetite is dissolved in the solution.

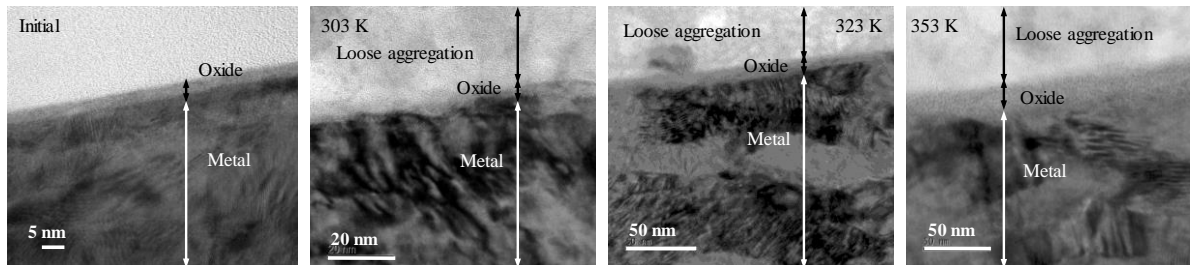


Figure 3.3.1: TEM observation of the surface oxide after two years of immersion in an NaOH solution at 303 K, 323 K and 353 K [SAKURAGI et al., 2016 b].

Table 3.3.1: Thickness of the oxide film in NaOH solution obtained from hydrogen generation (x) and by TEM observation

Temp. (K)	Test time (days)	x (nm)	Oxide thickness by TEM (nm)
303	720	2.61	2 - 4
	90	2.4	2 - 4
323	360	5.7	4 - 7
	720	10.2	5 - 10
353	720	27.1	7 - 14

Detailed analyses for the oxide at 303 K together with EDX and electron diffraction are shown in Figure 3.3.2. The cross section image might be constructed in three parts. The outermost surface (Point 1), appearing in heterogeneous light grey, consists of a silicon rich oxide mixture that might be loosely stitched and aggregated onto the surface oxide. The silicate is a dissolution product of the glass vessel. The silicate aggregation is also observed in the elemental distribution by XPS (Figure 3.3.3). Unless the Si precipitate is compacted, the effect of the loose aggregation on the corrosion resistance is considered to be negligible.

The second surface located on the metallic phase (Point 2) is an oxide that is generally referred to as a passive film. The oxide consists of iron, chrome and nickel, and is amorphous. Although the experimental condition is different, several oxides such as NiO and FeCr₂O₄ [BHATTACHARYA and SINGH, 2011] or Cr₂O₃ [LAYCOCK et al., 1995] were observed at the surface. However, it is not clear in the present work whether there is any formation of magnetite or chrome based passive oxide. The electron diffraction at 323 K and 353 K after 2 years in the NaOH solution also resulted in an amorphous structure.

Figure 3.3.3 shows the elemental composition and depth distribution of the oxide as measured by XPS. The initial oxide thickness is less than 10 nm, roughly corresponding to the TEM observation. The slight discrepancy of the oxide thickness results between the TEM and XPS methods may be attributable to the influence of surface roughness and sputter rate correction. After corrosion occurs, an Si-rich region appears which is approximately 30 nm to 50 nm at 303 K. This region corresponds to the loose aggregation shown in Figure 3.3.2 and expands with temperature. Because the oxide composition is not clearly determined by XPS in the profile, it is difficult at present to identify the characteristics and role of the oxide film that was formed under the temperature less than 353 K. Detailed analysis for the characterization of oxide is expected to be subject for further study.

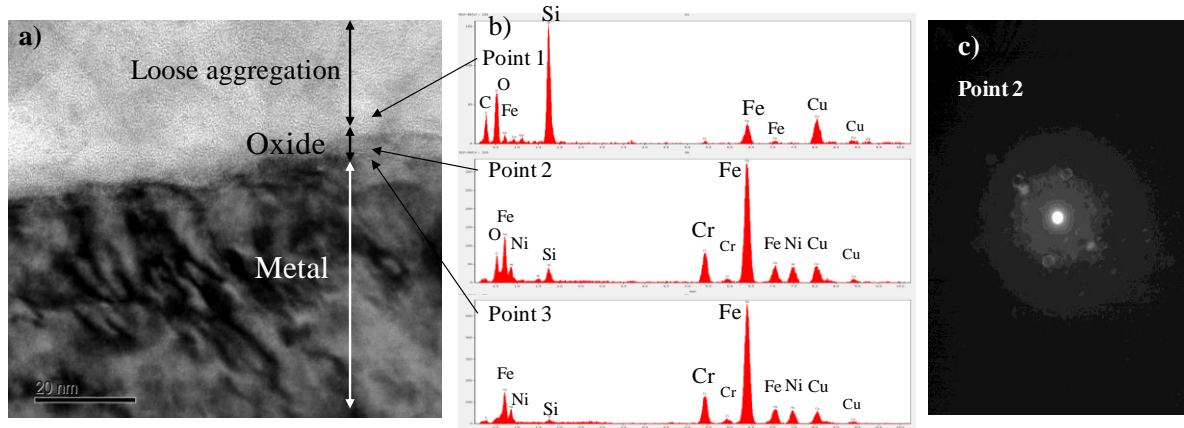


Figure 3.3.2: TEM observation of the surface oxide after two years of immersion in an NaOH solution at 303 K, and the corresponding b) EDX spectra and c) electron diffraction [SAKURAGI et al., 2016 a].

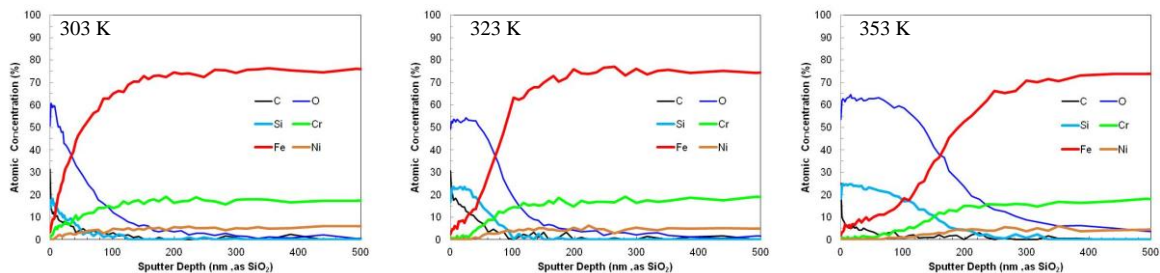
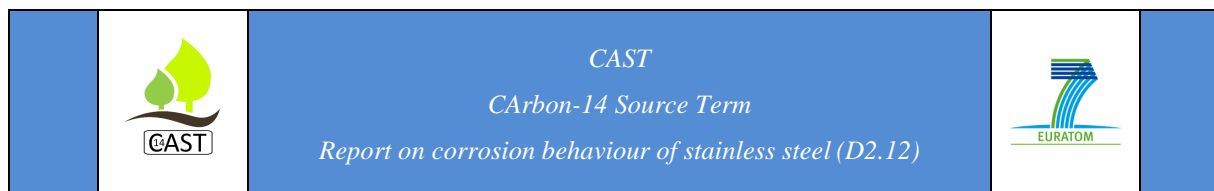


Figure 3.3.3: Depth profile of elements after two years of immersion in an NaOH solution by XPS measurement.

4 Conclusion

This report presents the corrosion behaviour of stainless steel in simulated deep repository water by evolved hydrogen measurement. The time dependence of the corrosion shows a parabolic rate law during one year from the start of test, of which activation energy is found to be 82.5 ± 6.2 kJ/mol. This corresponds to the energy for high temperatures down to 423 K and the process is under diffusion control. After the corrosion of two years the kinetics follows a linear rate law over the long term up to 6.5 years. The long term corrosion rate is approximately 0.4 nm/y at 303 K. This corrosion rate slower at 1/50 times the rate used in the conventional evaluation and will affect the estimation of radionuclide leaching and gas



generation for the safety assessment of stainless steel disposal of waste. This result, however, has not yet been thoroughly explained with respect to oxide film characteristics. The passive film is not clear because the oxide is very thin and amorphous. Silicon contaminants due to the dissolution of glass vessel under alkaline conditions make the oxide analysis more difficult. The detailed characteristics and role of the oxide film is expected to be subject for further study.

Acknowledgement

This research is a part of the “Research and development of processing and disposal technique for TRU waste” program funded by the Agency for Natural Resources and Energy in Ministry of Economy, Trade and Industry of Japan.

References

- ATOKINSON, A. 1985, Transport Processes during the Growth of Oxide Films at Elevated Temperature, *Reviews of Modern Physics* 57, 437-470.
- BHATTACHARYA, A and SINGH, P. M. 2011. Electrochemical behaviour of duplex stainless steels in caustic environment, *Corrosion Science* 53, 71-81.
- International Atomic Energy Agency (IAEA), 1998. Durability of Spent Nuclear Fuels and Facility Components in Wet Storage, IAEA-TECDOC-1012, Vienna.
- Federation of Electric Power Companies (FEPC) and Japan Atomic Energy Agency (JAEA), Second Progress Report on Research and Development for TRU Waste Disposal in Japan, JAEA AND FEPC REPORT TRU-2, 2007.
- HONDA, A. NISHIMURA, T., WADA, R., TANABE, M. 1999. Long Term Testing System, Testing Container and Measurement Container, Japan Patent 2912365.

LAYCOCK, N. J., NEWMAN, R. C., STEWART, J. 1995. The transpassive corrosion of stainless steel in stabilized alkaline peroxide solution, *Corrosion Science* 37, 1637-1642.

MAEKAWA, T., KAGAWA, K., NAKAJIMA, N. 1968. Corrosion Behavior of Stainless Steel in High-temperature Water and Superheated Steam, *Trans. JIM* 9, 130-136.

ROBERTSON, J. 1991. The Mechanism of High Temperature Aqueous Corrosion of Stainless Steels, *Corrosion Science* 32, 443-465.

SAKURAGI, T., MIYAKAWA, H., NISHIMURA, T., TATEISHI, Y. 2012. Corrosion Rates of Zircaloy 4 by Hydrogen Measurement under High pH, Low Oxygen and Low Temperature Conditions, *Mater. Res. Soc. Symp. Proc.* 1475, 311-316.

SAKURAGI, T., TANABE, H., HIROSE, M., SAKASHITA, A., NISHIMURA, T. 2013. Estimation of Carbon 14 Inventory in Hull and End-Piece Wastes from Japanese Commercial Reprocessing Operation, *Proceedings of the ICM2013*. Brussels, Belgium.

SAKURAGI, T., YOSHIDA, S., KATO, O., TATEISHI, Y. 2016a. Study of stainless steel corrosion by hydrogen measurement under deoxygenated, low-temperature and basic repository conditions. *Progress in Nuclear Energy* 87, 26-31.

SAKURAGI, T., YOSHIDA, S., KINUGASA, J., KATO, O., TATEISHI, Y. 2016b. Corrosion Kinetics of Stainless Steel by Hydrogen Measurement under Deep Geological Repository Condition. *Proceedings of Waste Management 2016 Conference*.

SAKURAGI, T. in prep. CAST WP Report-RWMC (D3.19), CAST Project Report.

SWANTON, S.W., BASTON, G.M.N., SMART, N.S. 2015, Rates of steel corrosion and carbon-14 release from irradiated steels – state of the art review (D2.1), CAST Project Report.